IEEE Access
Multidisciplinary | Rapid Review | Open Access Journal

Received April 21, 2019, accepted July 4, 2019, date of publication July 10, 2019, date of current version July 29, 2019.

Digital Object Identifier 10.1109/ACCESS.2019.2927747

Optimization Method of IR Thermography Facial Image Registration

BO-LIN JIAN[1], CHIEH-LI CHEN[2], (Senior Member, IEEE), CHIH-JER LIN[3], (Member, IEEE), AND HER-TERNG YAU[1], (Senior Member, IEEE)

[1]Department of Electrical Engineering, National Chin-Yi University of Technology, Taichung 41170, Taiwan
[2]Department of Aeronautics and Astronautics, National Cheng Kung University, Tainan 70101, Taiwan
[3]Graduate Institute of Automation and Technology, National Taipei University of Technology, Taipei 10608, Taiwan

Corresponding author: Her-Terng Yau (htyau@ncut.edu.tw)

This work was supported in part by the Ministry of Science and Technology of the Republic of China, Taiwan, under Contract MOST 107-2218-E-167 -004.

ABSTRACT So far, there have been many types of researches subject to technical requirements due to image registration. Using image registration can lower deviation from sequential images and make it possible to analyze the information variation of the particular area subsequently. This study provides a procedure creating fixed image based on the data of facial IR thermography, where its methods include the visual saliency map by detected image, as well as cluster algorithm. Comparison is also made here to solve the merits and demerits by affine parameter to reach the optimum measure among Genetic Algorithm, Particle Swarm Optimization, and Simulated Annealing Algorithm, where there are two control parameters concerning this experiment: one is the calculation of time confined each alignment, while the other one is to use parallel computing toolbox or not. The optimum method will be chosen by the values of the objective function based on the control parameters. Afterward, the optimal internal parameter is to be verified through the Taguchi experiment and the validity of this procedure in this study will be built following the parameter result as above. Therefore, the difference of images before and after alignment can be validated by overlapping the images before and after alignment as well as the image quality measurements, where its results reveal that the alignment procedure of IR thermography in this study is capable of performing human face alignment precisely, and subsequently, do help data statistics and analysis concerning temperature area interdependence.

INDEX TERMS Infrared thermography, image registration, genetic algorithm, particle swarm, simulated annealing algorithm, Taguchi method.

I. INTRODUCTION

Although there are still certain technical issues that need to be solved concerning luminance variation and facial gesture [1]–[3], researches of face detection via visible light have been developed and have come to many eminent conclusions in recent years, especially in the field of Deep Neural Networks (DNN) [4]–[6]. Generally, image data from visible light are under the influence of luminance variation profoundly on the visual environment, hence many studies have commenced with improvement of luminance influence by conducting IR thermography.

IR thermography instruments are usually applied to assist medical diagnosis in the medical science field. For example, to record temperature distribution and variation around eyeball [7], to estimate consumer's reaction through facial temperature data [8], to testify influence to the human body from battery heating [9], or to monitor temperature variation of the human forehead whilst we enter meditation [10]. In addition, research of human face detection is also a hot spot during recent years. Singh and Arora have proposed an algorithm subject to the feature-area [11] of auto-segmented profile in thermography, as well as finding paranasal sinus area on front face [12]. Also, Albarran et al., have proposed a thermography detection system of facial expression for anger, loathe, fright, joy and sorrow. Mostafa et al. [13], Budzan et al. [14] have proposed image processing and positioning for the face and two eyes under low resolution. Besides static IR thermography, researches are conducted too using dynamic image samples [14]–[17], where its application includes biotelemetry and face detection. Requirements subject to IR thermography alignment vary in accordance

The associate editor coordinating the review of this manuscript and approving it for publication was Mustafa Servet Kiran.

with different study purposes [18]. Müller et al., estimate the diversities between feature alignment and intensity alignment in thermography alignment [19], while Nico et al., attempt to perform alignment by thermography and MRI [20]. Though alignment process of face IR thermography is a very important topic among all those researches, yet there is still a leaking of numerous discussions for IR thermography. It is rather substantial of sequential image registration whilst collecting IR thermography of the human face, because testers must be accommodated under somehow a natural and easy condition without fixing their heads, which makes it harder to analyze subsequent relevance.

Image registration can be divided through method into feature and area. Eye positioning is an important index [13] by the former. 86% of the accuracy of human eye positioning can be approached through the Adaboost algorithm provided by Wang et al. [21]. Although the study described above is a tool for eye positioning, feature differences do not come out clearly. Besides, image registration based on feature method is not applicable to any circumstance with higher nonlinear difference [22], [23], plus Adaboost [24], [25] positioning needs a numerous training samples, whilst precise eye position is not easy to acquire by gray value projection algorithm [26], [27]. For the solution Jian and Chen had once proposed a semi-automatic procedure to fabricate fixed image [28] by using eye look and geometric data, and apply alignment by the area principle. Alignment based on area measure is usually solved via optimization method [29], [30]. Although there have been many experts engaged in concerned researches, it is always difficult to reach the best solution amongst all these multitudinous optimization methods because the choosing of corresponding internal parameters must be taken into consideration, furthermore, application to different fields [31]–[33] is also the cause. Due to that the image sample for this study is the human face by IR thermography, plus affine parameters are suitable to distinguish differences between those images, we herein adopt affine parameters [28], [34] to be as our alignment parameters of every image. The purpose of this research using equivalent type sample is to launch the discussions about how to create fixed image automatically, what the best optimization algorithm is, how to adjust the best internal parameter and what quality of image registration.

II. METHODS

This study launches an experiment by collecting facial images of IR thermography to establish a database, and to find the best alignment parameter via optimization method to correct every sequential image under the condition of not fixing testers' heads. First, environmental and instrumental configurations are explained in experimental setup section. Jian and Chen had provide a procedure of fabrication fixed image which can be adapted to IR thermography for the human face [28] once. Even if this solution does answer the problem of accuracy for eye positioning, it still needs to manually pick up the rough position of the eye to fabricate a fixed image in practical situation. Therefore, in use of extract salient regions in fabricating fixed image section in this study provides an improved process to make fabrication of fixed image wiser and more automatic. In evaluation of optimization method for thermal facial image sequences section indicates that we can use Genetic Algorithm (GA), Particle Swarm Optimization (PSO) and Simulated Annealing Algorithm (SAA), as well as adopting normalized mutual information (NMI) as objective function, to calculate similarity between fixed image and moving image in order to align unintentional minor rotation. It is the same section where explains design of Taguchi's Orthogonal Arrays and Signal-to-Noise (S/N) Ratio. In diversities of fixed images subject to different methods section the results of fixed image from this research are shown and compared with those images using traditional methods. In comparison between each optimization method of thermal face image registration section maximum alignment time for single image is to be limited, and differences of objective function through various optimization methods of alignment will be compared. In addition, diversities before and after using parallel computing toolboxes will also be put into discussion. In parameters choice for PSO optimization method section Taguchi Methods are conducted to solve the optimum alignment parameter and verify the results more efficiently. In relative analysis between fixed image frame and alignment quality section, overlapped images before and after alignment, as well as numerical results quantified by image quality evaluation index before and after aligning, will both be discussed is.

A. EXPERIMENTAL SETUP

A temperature distribution matrix on human facial skin is built by Digital Infrared Thermal Image System (DITIS - Spectrum 9000-MB Series; United Integrated Service Compny Ltd). Where its resolution from temperature data collected via IR thermography of the human face is a 320 × 240 matrix, sampling frequency is 2 fps. DITIS specification is shown in Table 1.

TABLE 1. Milling parameters.

IR sensor type	Micro bolometer
Noise equivalent temperature difference	0.07°C
Temperature measurement range	10°C to 40°C
Image resolution	320(h) × 240(v)

DITIS is used to shoot thermal radiation status. In order to prevent any other heat sources from interfering accuracy of this experiment or damaging IR thermography of the human face, it is necessary to lower any influence from other thermal interference as possible as we can. Environmental temperature must remain within 26°C to 28°C in sampling process. Also, irrelevant personnel are forbidden to walk around the spot in the cause of prevention from strong heat convection. In addition, three-layer blackout fabric is used to surround the environment, making sure that reflection factor of thermal radiation will be minimized.

Process of image collecting is make tester watch a video clip lasing 8 minutes and 50 seconds, where the clip is compiled by IAPS [35] image. Temperature distribution matrix data will be gathered by DITIS from the tester provoked by IAPS, and there are 1060 frames gathered in total per sampling. Machine or instrument will be adjusted in advance every time before sampling, ensuring tool stability for thermography information, as well as that complete face image by IR thermography and proper space margin can be obtained. PC hardware specification for this study is Intel(R) Core(TM) i9-9820X CPU 3.30 GHz, RAM 32 GB. Where the verification software is MATLAB 2018b, and the toolboxes in use are Optimization Toolbox and Parallel Computing Toolbox.

B. USE OF EXTRACT SALIENT REGIONS IN FABRICATING FIXED IMAGE

Intention of fixed image is to establish a criterion which can be the basis of alignment for each subsequent image; even more, results of fixed image production will do affect the alignment of sequential images. Hence, method of using the first image to fabricate fixed image is launched to make comparison with traditional measure. The process is shown in Figure 1.

Saliency Detection Algorithm [36] provided by Rahtu and Heikkilä is a method based on a probabilistic

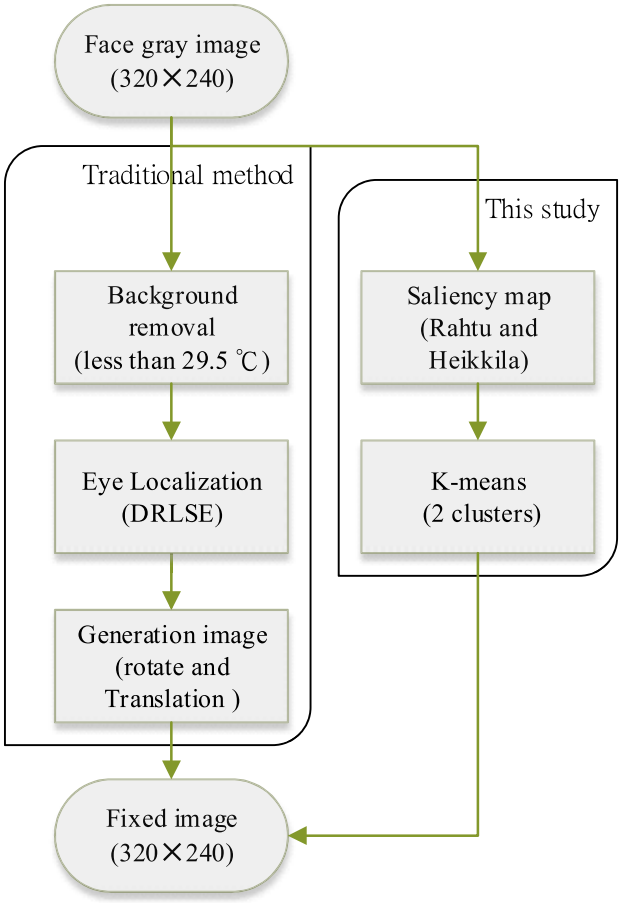

FIGURE 1. Fixed image processing flow chart. Left side: Traditional method; Right side: Method in this study.

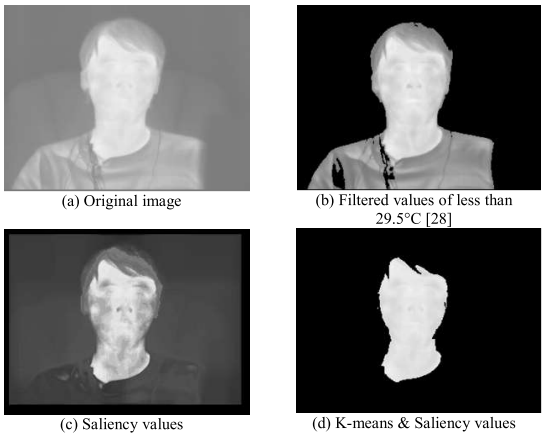

FIGURE 2. Example of traditional method [28], saliency detection [36] and saliency detection & K-means, using single scale and image intensity values as features: (a) Original image; (b) Filtered values of less than 29.5°C; (c) Saliency values; (d) K-means & Saliency values.

interpretation of the semilocal feature contrast. Comparison is made here between this method and traditional background threshold [28] in order to estimate advantage of the former. Original image is shown in Figure 2 (a). The threshold of traditional method is 29.5°C, any temperature value less than this threshold is configured as zero. The threshold covers facial temperature, therefore we can use it to filter other temperature interference due to background or environment; the result image is shown in Figure 2(b). Result image by applying the method from Rahtu and Heikkilä [36] is shown in Figure 2(c). K-means [37] is conducted to segment result images automatically after saliency map is detected. According to information differences between foreground and background, we can easily spot thermography data of facial area, where the result from automatic process is shown in Figure 2(d). In diversities of fixed images subject to different methods section, diversities between traditional method and this study shall be discussed.

C. EVALUATION OF OPTIMIZATION METHOD FOR THERMAL FACIAL IMAGE SEQUENCES

Optimization algorithm of GA, PSO, SA are conducted in this study to solve Affine Transformation parameters. Alignment criterion applied to fixed image and moving image is Normalized Mutual Information (NMI), wherein image content of Affine Transformation comprises translation, scale, shear and rotation. And the transformation formulas are defined as form (1) and (2) [38]:

$$\underbrace{\begin{bmatrix} x_{n2} \\ y_{n2} \\ 1 \end{bmatrix}}_{\mathbf{I_{n2}}} = \underbrace{\begin{bmatrix} 1 & 0 & p_x \\ 0 & 1 & p_y \\ 0 & 0 & 1 \end{bmatrix}}_{\mathbf{T_{translation}}} \underbrace{\begin{bmatrix} \cos(\theta) & -\sin(\theta) & 0 \\ \sin(\theta) & \cos(\theta) & 0 \\ 0 & 0 & 1 \end{bmatrix}}_{\mathbf{R_{rotation}}} \cdots \underbrace{\begin{bmatrix} p_s & 0 & 0 \\ 0 & p_s & 0 \\ 0 & 0 & 1 \end{bmatrix}}_{\mathbf{S_{scale}}} \underbrace{\begin{bmatrix} 1 & p_{sx} & 0 \\ p_{sy} & 1 & 0 \\ 0 & 0 & 1 \end{bmatrix}}_{\mathbf{S_{shear}}} \underbrace{\begin{bmatrix} x_{n1} \\ y_{n1} \\ 1 \end{bmatrix}}_{\mathbf{I_{n1}}} \tag{1}$$

$$\mathbf{I_{n2}} = \mathbf{T_{translation}}\mathbf{R_{rotation}}\mathbf{S_{scale}}\mathbf{S_{shear}}\mathbf{I_{n1}} \quad (2)$$

(x_{n2}, y_{n2}) : image coordinate after alignment; p_x: shift value among x axis; p_y: shift value among y axis; θ: angle of rotation in the center; p_s: image scaling magnification; p_{sx}: shear value among x axis; p_{sy}: shear value among y axis; (x_{n1}, y_{n1}): image coordinate before alignment.

A similarity index [39]–[41] of NMI is usually used as objective function in image registration, where the higher the resulting value is, the better the two images overlap. Herein MATLAB toolbox is selected to be the optimization method, and the default objective function to be solved here is to search for the minimum value mainly. For the sake of convenient computation, a minus sign is added in front of the NMI formula, the lower of the value is the better, as shown in form (3):

$$\mathbf{NMI}(\mathbf{I_f}, \mathbf{I_m}) = -\frac{\mathbf{H}(\mathbf{I_f}) + \mathbf{H}(\mathbf{I_m})}{\mathbf{H}(\mathbf{I_f}, \mathbf{I_m})} \quad (3)$$

$\mathbf{H}(\mathbf{I_f})$ and $\mathbf{H}(\mathbf{I_m})$ are the marginal entropies of fixed and moving images;

$\mathbf{H}(\mathrm{I_f}, \mathrm{I}, \mathrm{m})$ is the joint entropy of fixed and moving images.

In order to compare advantages and disadvantages amongst each method, the same parameter searching range is applied to diverse methods. In this research, range limitation configurations for the six alignment parameters of Affine Registration are shown in Table 2.

TABLE 2. Limitation for parameters searching range of affine registration.

Parameters	Minimum	Maximum
p_x	–5 pixel	5 pixel
p_y	–5 pixel	5 pixel
p_s	0.9	1.1
p_{sx}	–0.01	0.01
p_{sy}	–0.01	0.01
θ	-5^o	5^o

There are numerous optimization methods, wherein GA is an imitation of ''survivor of the fittest'' from Darwin's Theory of Evolution, which was at the earliest proposed by professor Holland in the university of Michigan. Until today, GA has been applied to and verified by many different fields [33], and is the very important method in solving global optimization. On the other hand, PSO is a solution proposed by Eberhart and Kennedy based on the foraging of bird groups. Because PSO has many merits such as easiness, convenient to accomplish and less parameter configuration, it has become quite popular recently in application to many researches [33]. Also, main theory of SAA is in accordance with annealing process, comprising heating, isothermal and cooling processes. This method has achieved great success in solving the design for circuit layout of Travelling Salesman Problem (TSP) and Super-Large-Scale Integration (SLSI). Processing flow chart for the three optimization methods

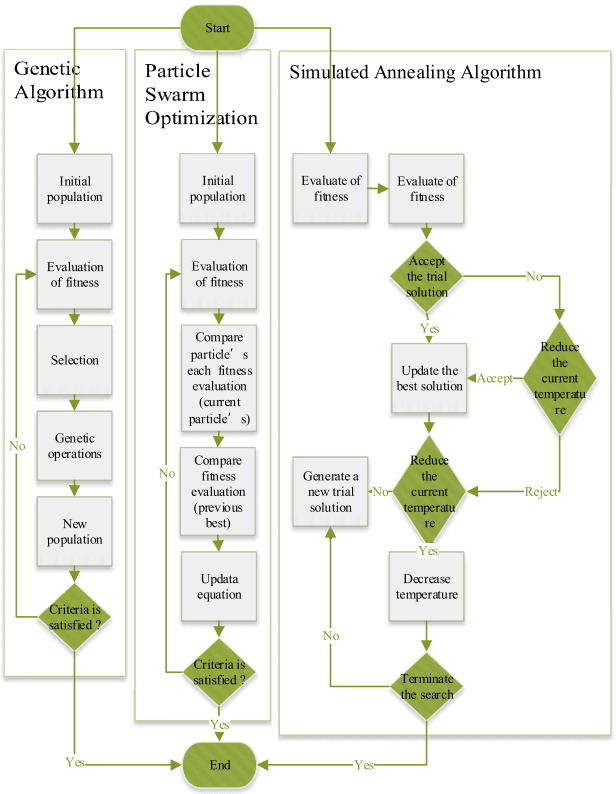

FIGURE 3. Diagram of optimization methods by GA, PSO and SAA. Left side: GA flow chart; Middle: PSO flow chart; Right side: SAA flow chart.

above to function is shown in Figure 3. In order to distinguish advantages and disadvantages of thermography alignment between these three famous optimization methods, as well as to make a detached system where the results will not be deviated due to programming capacity, toolbox is conducted here to approach GA [42]–[44], PSO [45]–[47] and SAA [48]. Alignment measure and evaluation procedure in this study are both shown in Figure 4. Furthermore, comparison of the experiment results shall be explained from comparison between each optimization method of thermal face image registration section to relative analysis between fixed image frame and alignment quality section.

After confirming the fittest optimization algorithm in accordance with the results in comparison between each optimization method of thermal face image registration section experiment, we still need to acquire the internal parameters for the algorithm. Taguchi Methods are founded by PhD Genichi Taguchi, which its main purpose is to streamline experiment frequency and to improve method for data analysis. Nevertheless, among all those optimization methods, parameter adjustment can only rely on assumption or the rule of thumb in the past, but now a more systematic method can be added to evaluate parameter. In this study, we introduce Taguchi Methods to record and analyze the values of objective function, and choose the optimization conditions in an objective way in order to take cost into account as well as to find out consequences between those parameters.

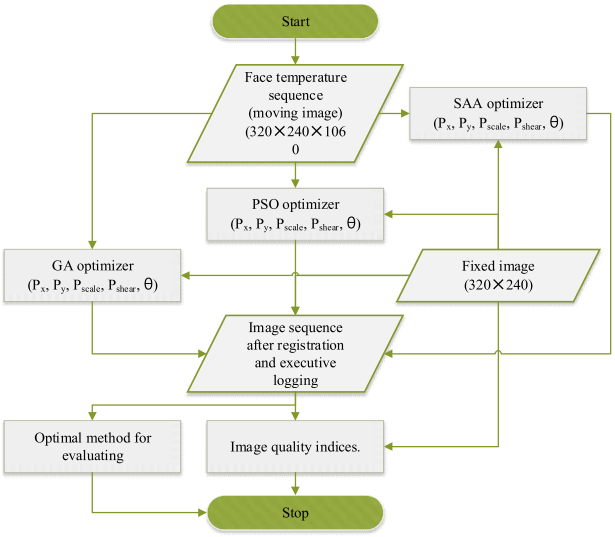

FIGURE 4. Alignment Method and Evaluation of This Study. Alignment includes optimization methods of GA, PSO and SAA; evaluation includes image quality index and overlapping condition.

There are some other researches in different fields to be applied with the concerning methods mentioned in this study as well [49]–[51]. In this research, Taguchi experiment is selected to decide internal parameters of optimization methods. The two main tools in Taguchi Methods are orthogonal arrays as well as S/N ratio. The point of this study lies on how to reduce variation from experiment results and to solve optimization parameter sets, as well as to obtain the optimum parameters for affine registration. S/N ratio can be calculated and solved in accordance with the parameter sets of Taguchi's Orthogonal Arrays. "Relative deviation" is adopted in this study, which means S/N ratio, herein referred as S/N_{NB3}, is obtained through standard deviation divided by average; herein S/N_{NB3} is shown in from (4) to (5):

$$S/N_{NB3} = -10 \times \log\left(\frac{S^2}{\bar{y}^2}\right) \tag{4}$$

$$S = STD(\mathbf{Data}_i) \tag{5}$$

$$\bar{y} = AVG(\mathbf{Data}_i) \tag{6}$$

wherein *STD* is the function for solving standard deviation. $\mathbf{Data}_i$ is the result of image registration of objective function, where the subscript i indicates the image number $i(i = 1, 2, \ldots, 1060)$. For the easier comprehension, herein $\mathbf{Data}_i = -\mathbf{NMI}(\mathbf{I_f}, \mathbf{I_m^i})$. *AVG* is the function for solving average. When we apply this formula to calculate S/N ratio, it means repeatability of the experiment results is poor if the value of S is larger; on the contrary, repeatability will be better if S is smaller. Based on the formula definition in this study, the larger S/N_{NB3} is, the more reliable the experiment results are. Eventually, after we solve S/N_{NB3}, a factor effects chart can be computed respectively. Then we can decide the optimization parameters with best stability on the basis of factor effects diagram, wherein the larger the value shown in factor effects diagram is the fitter being optimization parameter it is.

Experiment results are described in parameters choice for PSO method section. At last, divergence is put into discussion before and after alignment in relative analysis between fixed image frame and alignment quality section, and the results are evaluated through overlap method and quality measurement index.

III. RESULTS AND DISCUSSIONS

A. DIVERSITIES OF FIXED IMAGES SUBJECT TO DIFFERENT METHODS

In the past, traditional semi-automatic measure [28] was performed by an operator picking the rough position of the human eye, and then using the temperature deviation between the eye and facial skin to confirm the outline of both eyes via Distance Regularized Level Set Evolution (DRLSE) [52]. Then the Center of Mass of the Region can be computed by the outline of both eyes, and we can use this mass center to decide the quantity of rotation and shift, as shown in Figure 5 (a). The new method mentioned in use of extract salient regions in fabricating fixed image section is introduced to produce fixed image in this research, and the result is shown in Figure 2 (d). To investigate discrepancy in these two methods, we examine them for further analysis, as shown in Figure 5 (b). In this image, the green region is hair, which does not belong to the fixed image produced in this study, while it does on the contrary in using traditional method. Additionally, main color of the neck region is magenta; because fixed rectangular data processing is adopted in traditional method, it is not possible to compute the information about this region, but we do take this part of data into account in this study. In thermography image registration of the human face, temperature variation of the human body should be the main target for observation, and all the skin regions with temperature distribution can be spotted automatically by this research. Therefore, a solution to the defect of using rectangles to form margins in those positions we are interested with is made, which can be more sophisticated in dealing with information.

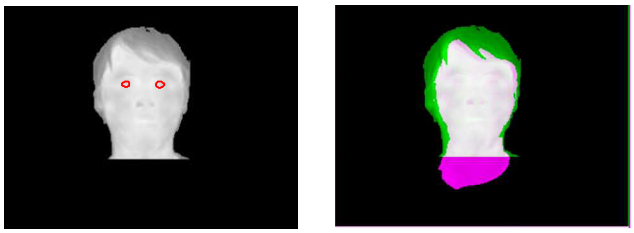

(a) Detected by traditional method [28, 53]

(b) Magenta and green regions show where the intensities are different between this study and traditional method.

FIGURE 5. Template of image results by traditional method and this study. (a) Detected by traditional method; (b) Magenta and green regions show where the intensities are different between this study and traditional method.

B. COMPARISON BETWEEN EACH OPTIMIZATION METHOD OF THERMAL FACE IMAGE REGISTRATION

It is difficult to compare each optimization method because the results varies by convexity and concavity of objective function and constraints. Hence, this study is subject to investigate the differences between GA, PSO and SAA methods under the limitation by using only thermal face image samples as well as restricting the maximum computation time for single image. In comparison between each optimization method of thermal face image registration section, toolbox default configuration is conducted mainly in the experiment of deciding optimization parameters. Variation of the objective function is observed in this experiment when we limit the maximum computation time for single image registration and decide to use parallel computing tools or not during the alignment processing with limitation for optimization methods. This comes as the results that the thresholds of maximum computation time are 5, 10, 15, 20 and 25 seconds, and the average results of 1060 frames are to be adopted to reduce deviation in study. The results are shown in Table 3 , where they are the variations of objective function by diverse computation times without using any parallel computing tool under the limitation for maximum computation time during image registration by using optimization methods. As we see in Table 3, performance of GA is the best, then PSO, and SAA is the worst. And even we assess the objective functions by maximum computation time limited subject to respective observation, performance of GA is still the best, whilst PSO is worse than SAA under 10-second limitation only but better than any other result. Table 4 uses the same test process as Table 3 does, but parallel computing tool is added here to accelerate the efficiency, and the results are shown in Table 4. To make this estimation more objective, we apply the commercial program to make comparison; yet SAA method is not compatible with parallel computing toolboxes, so the results of SAA method is excluded in Table 4. As the conclusion of Table 4, performance of PSO is better than GA in summary. Objective function results of PSO perform better than GA under the limitation of maximum computation time subject to respective observation, except the results of 5-second computation. From Table 3 and Table 4, we know we can acquire the best solution for the objective function substantially under limited time as long as we use parallel computing toolboxes. The results subject to 5-second computation time in Table 4 are better than any result coming from any limited computation time in Table 3. Of course, these results also depend on different hardware specifications. Suggestion is made for researchers to use GA for solving image registration under the circumstance of not using parallel computing tools in thermal face image. On the other hand, if parallel computing tools are adopted under the same sampling conditions, we will recommend researchers to adopt PSO for solution. The results in Table 4 have shown the numerical variations are diverse. To watch the variations more conveniently, we use the PSO results in Table 4 to make a diagram as shown in Figure 6. The limited maximum computation time for each PSO image is indicated on x axis in Figure 6, whilst the values of objective function corresponds to y axis; the blue line means connection between each raw datum in straight line, and the green shows results of cubic embedding. An obvious truth is that the objective function has the largest variation under the limitation of 10-second computation no matter whether they are PSO raw data or embedded results. Hence, stop the condition subject from adopting 10 seconds as computation time for a single image would be more efficient under the circumstance using parallel computing toolboxes in this study.

TABLE 3. Results of objective function of GA, PSO and SAA under limitation of maximum computation time for single image.

	Time (sec)					
	5	10	15	20	25	Avg.
GA	-0.2644	-0.2642	-0.2703	-0.270178	-0.2746	-0.2687
PSO	-0.2514	-0.2582	-0.2638	-0.2671	-0.2707	-0.2622
SAA	-0.2468	-0.2589	-0.2619	-0.2642	-0.2661	-0.2596

Note：
1. Results in this table are the averages of objective function (such as form (3)) for solution of 1060 frames.
2. Without parallel computing toolbox.
3. Optimum internal parameters are adopted by using software default.

TABLE 4. Results of Objective function of GA, PSO and SAA under Limitation of Maximum Computation Time for Single Image (using parallel computing toolbox).

	Time (sec)					
	5	10	15	20	25	Avg.
GA	-0.2773	-0.2832	-0.2845	-0.2853	-0.2859	-0.2832
PSO	-0.2764	-0.2906	-0.2919	-0.2922	-0.2922	-0.2887

Note：
1. Results in this table are the averages of objective function(such as form (3)) for solution of 1060 frames.
2. Using parallel computing toolbox.
3. Optimum internal parameters are adopted by using software default.

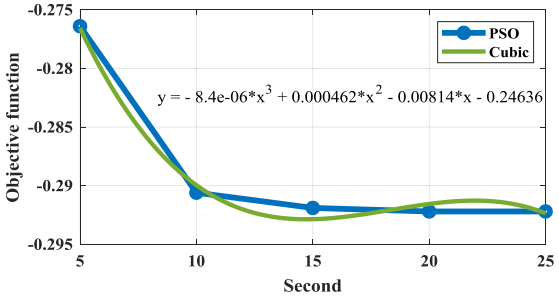

FIGURE 6. Diagram graphs of stop condition by time and objective function.

C. PARAMETERS CHOICE FOR PSO OPTIMIZATION METHOD

The results are shown in comparison between each optimization method of thermal face image registration section that best efficiency can be reached if we configure stop condition

TABLE 5. Taguchi's orthogonal arrays and computing results of PSO parameter adjustment.

Exp.	Inertia range	Self-adjustment Weight	Social-adjustment weight	Swarm size	S / N ratio
1	[0.1 1.1]	1.49	1.49	60	63.4352
2	[0.1 1.1]	1.69	1.69	120	154.5305
3	[0.1 1.1]	1.89	1.89	180	165.3216
4	[0.05 1.05]	1.49	1.69	180	157.7740
5	[0.05 1.05]	1.69	1.89	60	173.0525
6	[0.05 1.05]	1.89	1.49	120	155.1837
7	[0.15 1.15]	1.49	1.89	120	154.2474
8	[0.15 1.15]	1.69	1.49	180	168.2482
9	[0.15 1.15]	1.89	1.69	60	180.7952

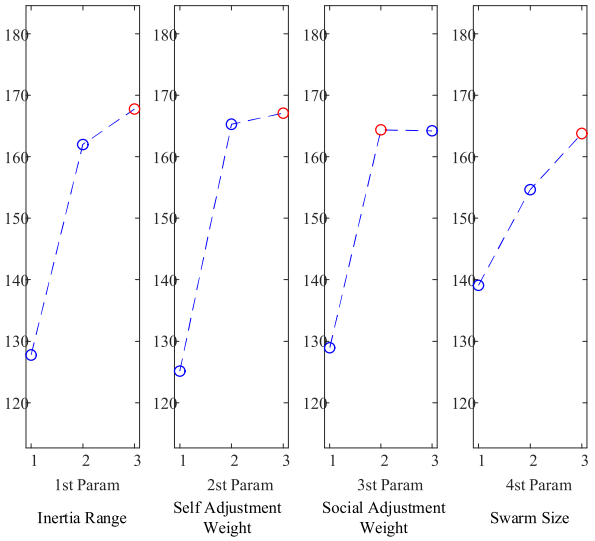

FIGURE 7. Factor effects diagram.

TABLE 6. Optimum PSO parameter configuration by best factor and significance level.

Factor	Best Level
Inertia Range	[0.15 1.15]
Self-adjustment Weight	1.89
Social-adjustment Weight	1.69
Swarm Size	180

1. Objective function value -0.3379 can be obtained by using the parameter set above.
2. Results in this table are the averages of objective function (such as form (3)) for solution of 1060 frames.
3. Using parallel computing toolbox.
4. Limitation for computing time is 10 seconds.

by 10 seconds for a single PSO image registration when we use parallel computing toolbox. Therefore, we would like to find the optimum parameter set for PSO method under the same conditions, and Taguchi Methods as mentioned above in evaluation of optimization method for thermal facial image sequences section will be used here to be the basis for this choice. Table 5 shows $L_9(3^4)$ as the Taguchi's Orthogonal Arrays were used in this study; wherein the subscript indicates times of experiment, the numeral "3" in brackets means there are three significance levels for each factor, and the superscript "4" means 4 factors are involved here. Inertia is the vital one among all PSO parameters; if the absolute value of inertia is higher, new computing speed generated will also become faster at the same time. Nevertheless, if the absolute value of inertia goes higher, then group stability will worsen; so it is relevantly important to configure inertia weight and limit its range. In this research, configuration for inertia range is launched to be the first factor put into discussion, the ranges under our consideration are 0.1 to 1.1, 0.05 to 1.05 as well as 0.15 to 1.15. The second factor will be self-adjustment weight of inertia; as being an attraction to the best location where particle has visited, we consider influences to PSO under the configurations as 1.49, 1.69 and 1.89. The third factor is social-adjustment weight, which its function is to make the particle head more toward the best place in the current neighborhood. Discussion is made about influences to PSO under the configurations as 1.49, 1.69 and 1.89. The last factor is swarm size, which indicates particle numbers for each time. The higher the configuration is set, the larger quantity the particle has; also, we can attain a more precise solution under the prerequisite of sacrificing computation speed. Herein they are configured as 60, 120 and 180. As a summary above, there are four factors and three different significance levels in total. Optimum S/N ration can be referred through Taguchi Methods, and calculations of $L_9(3^4)$ as the Taguchi's Orthogonal Arrays for PSO parameter adjustment are shown in Table 5. Where the results show that the optimum one in this experiment as S/N ratio corresponds to is the 9th. In order to further investigate each significance level of the chosen factors, factor effects diagram is conducted here for respective analysis, which is shown in Figure 7.The factor effects diagram is a graph expressing effect of each factor, with the horizontal axis representing the level of the factor and vertical axis representing the S/N ratio and the characteristic value. From this graph, we can find the condition with higher S/N ratio and select the one with better characteristics. According to the results in Figure 7, the optimum significance level for each factor can be approached, i.e. the largest values as well as those symbols of red circle. The optimum results are as below: 3rd level [0.05 1.05] of the 1st factor, 3rd level 1.89 of the 2nd factor, 2nd level 1.69 of the 3rd factor and 3rd level 180 of the 4th factor. The optimum parameter set of PSO decided via the best factor and significance level is shown in Table 6. After then image registration of PSO will be performed again using the optimum level of each factor, as well as the same limitation for 10-second computing, we can acquire the average result of -0.3379 from our objective function based on 1060 frames. Comparison is

made here between Table 3 and Table 4, and now we find that the minimum value we seek here is far better than those ones use default after adjusting the parameter configuration. Efficiency of the optimum parameter through Taguchi Methods is astonishing if parallel computing tools are adopted by; also, solution precision will improve much more under limited computation time. Where its index of relative percent difference is improved from 14.51% (objective function result subject to 20-second limitation of PSO in Table 4) to 31.16% (objective function result subject to 5-second limitation of SAA in Table 3).

D. RELATIVE ANALYSIS BETWEEN FIXED IMAGE FRAME AND ALIGNMENT QUALITY

Alignment quality comparison between before and after image registration is made by overlapping two images as well as image quality measurement index in this study. Information of images aligned in sequence without other redundant data but only temperature concerning is shown in Figure 8. Also, image overlap comparison by two of the most divergent images is made in sequential image evaluation in accordance with Structural Similarity (SSIM) index, which its result is shown in Figure 9. Overlapped colors as magenta and green regions show where the intensities are different of frame 1 and 1060. Temperature areas in the body region overlapped in this graph almost match perfectly, and show no diversity of green or magenta. For more detailed comparison, we magnify the results as shown in the red-color and blue-color frames.

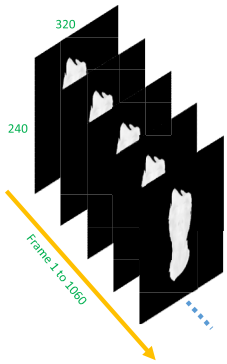

FIGURE 8. Exterior sketch after alignment.

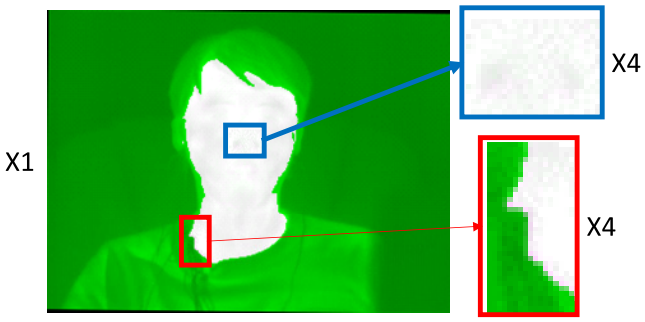

FIGURE 9. Comparison between two of the most divergent images. magenta and green regions show where the intensities are different.

TABLE 7. Statistical results for image quality indices.

Indices	Average (1060 frame)	
	Before Registration/ After Registration	Relative Percent Difference
$Quality_{PSNR}$	5.2327/5.3391	2.0129
$Quality_{MSE}$	19510/19036	2.4594
$Quality_{SSIM}$	0.1081/0.116	7.0504

Where the red frame indicates the most deviated part amongst the sequential images, whilst a slight divergence can be seen in the blue frame on nose with which we use to breathe. This kind of divergence of the later belongs to natural breathing, and it means the overlapping result here is almost flawless.

Additionally, we use image quality measurement index MSE (Mean Squared Error) [53]–[55], PSNR (Peak Signal to Noise Ratio) [53], [54] and SSIM (Structural Similarity Index) [56] to implement further analysis. Image quality measurement index is referred to fixed image, and other moving images are our targets. The formula is as (7):

$$Quality_{Type} = Q_{Type}(\mathbf{I_f}, \mathbf{I_m}) \tag{7}$$

Herein Q is the function for calculating image quality, and the subscript *Type* means there are three methods: PSNR, MSE and SSIM for calculation; $\mathbf{I_f}$ represents fixed image, and $\mathbf{I_m}$ represents moving image. Average results of the 1060 frames computed through form (6) before and after alignment are shown in Table 7, which show that the results after alignment are better. Formula of relative percent difference is the absolute value of difference from two values divided by the average of these two values, and then multiplies by 100%. Index results of relative percent difference in Table 7 have indicated that there is an improvement from 2% to 7%, especially SSIM index in which indicated 7%, has the upmost effect. Therefore, from the perspective on image overlap and quality index, the alignment method in this study is efficient.

IV. CONCLUSION

This study provides an automatic process for fabricating fixed image, and compares the advantages and disadvantages among Genetic Algorithm, Particle Swarm Optimization and Simulated Annealing Algorithm. Then we use Taguchi experiment and factor effects diagram to launch the significance level for each factor by optimum internal parameters. Also, the automatic process mentioned in this study can separate background and foreground of image. In addition, we have defined the optimal environmental configuration for GA and PSO when a comparison is made between these three optimization methods. At the same time, we also prove that computing efficiency can incredibly improve with the support of parallel computing toolbox. Afterwards we use Taguchi's Orthogonal Arrays to spot the optimum S/N ratio, and find out the optimal significance level for each factor via factor effects diagram. After the experiment of image registration

via the optimized internal parameters of PSO, we can see a tremendous improvement on relative percent difference from 14.51% to 31.16%, whilst the results of it in the Structural Similarity Index show an efficiency improvement of 7.05 %. Eventually, the conclusion is to be made here that the process of image registration in this study for IR thermography image of the human face is helpful to analyze subsequent analysis and all statistical researches concerned.

REFERENCES

[1] M. P. Beham and S. M. M. Roomi, "A review of face recognition methods," (in English), *Int. J. Pattern Recognit. Artif. Intell.*, vol. 27, no. 4, Jun. 2013, Art. no. 1356005.

[2] R. Gade and T. B. Moeslund, "Thermal cameras and applications: A survey," *Mach. Vis. Appl.*, vol. 25, no. 1, pp. 245–262, 2014.

[3] S. H. Abdurrahim, S. A. Samad, and A. B. Huddin, "Review on the effects of age, gender, and race demographics on automatic face recognition," (in English), *Vis. Comput.*, vol. 34, no. 11, pp. 1617–1630, Nov. 2018.

[4] J. Li, L. Liu, J. Li, J. Feng, S. Yan, and T. Sim, "Toward a comprehensive face detector in the wild," *IEEE Trans. Circuits Syst. Video Technol.*, vol. 29, no. 1, pp. 104–114, Jan. 2019.

[5] S. Yang, P. Luo, C. C. Loy, and X. Tang, "Faceness-Net: Face detection through deep facial part responses," *IEEE Trans. Pattern Anal. Mach. Intell.*, vol. 40, no. 8, pp. 1845–1859, Aug. 2018.

[6] H. Wu, K. Zhang, and G. Tian, "Simultaneous face detection and pose estimation using convolutional neural network cascade," *IEEE Access*, vol. 6, pp. 49563–49575, 2018.

[7] J. Pattmoller, J. Wang, E. Zemova, B. Seitz, T. Eppig, A. Langenbucher, and N. Szentmáry, "Correlation of corneal thickness, endothelial cell density and anterior chamber depth with ocular surface temperature in normal subjects," (in English), *Zeitschrift Medizinische Physik*, vol. 25, no. 3, pp. 50–243, Sep. 2015.

[8] C. G. Viejo, S. Fuentes, K. Howell, D. D. Torrico, and F. R. Dunshea, "Integration of non-invasive biometrics with sensory analysis techniques to assess acceptability of beer by consumers," (in English), *Physiol. Behav.*, vol. 200, pp. 139–147, Mar. 2019.

[9] J. Bauer, C. O'Mahony, D. Chovan, J. Mulcahy, C. Silien, and S. A. M. Tofail, "Thermal effects of mobile phones on human auricle region," (in English), *J. Therm. Biol.*, vol. 79, pp. 56–68, Jan. 2019.

[10] J. Singh, S. Kumar, and A. S. Arora, "Thermographic evaluation of mindfulness meditation using dynamic IR imaging," (in English), *Infr. Phys. Technol.*, vol. 95, pp. 81–87, Dec. 2018.

[11] J. Singh and A. S. Arora, "An automated approach to enhance the thermographic evaluation on orofacial regions in lateral facial thermograms," (in English), *J. Therm. Biol.*, vol. 71, pp. 91–98, Jan. 2018.

[12] J. Singh and A. S. Arora, "A framework for enhancing the thermographic evaluation on characteristic areas for paranasal sinusitis detection," (in English), *Infr. Phys. Technol.*, vol. 85, pp. 457–464, Sep. 2017.

[13] E. Mostafa, R. Hammoud, A. Ali, and A. Farag, "Face recognition in low resolution thermal images," *Comput. Vis. Image Understand.*, vol. 117, no. 12, pp. 1689–1694, 2013.

[14] S. Budzan and R. Wyżgolik, "Face and eyes localization algorithm in thermal images for temperature measurement of the inner canthus of the eyes," *Infr. Phys. Technol.*, vol. 60, pp. 225–234, Sep. 2013.

[15] G.-A. Bilodeau, A. Torabi, P.-L. St-Charles, and D. Riahi, "Thermal–visible registration of human silhouettes: A similarity measure performance evaluation," *Infr. Phys. Technol.*, vol. 64, pp. 79–86, May 2014.

[16] A. Torabi and G.-A. Bilodeau, "Local self-similarity-based registration of human ROIs in pairs of stereo thermal-visible videos," *Pattern Recognit.*, vol. 46, no. 2, pp. 578–589, 2013.

[17] C. K. Eveland, D. A. Socolinsky, and L. B. Wolff, "Tracking human faces in infrared video," *Image Vis. Comput.*, vol. 21, no. 7, pp. 579–590, 2003.

[18] R. S. Ghiass, O. Arandjelović, A. Bendada, and X. Maldague, "Infrared face recognition: A comprehensive review of methodologies and databases," *Pattern Recognit.*, vol. 47, no. 9, pp. 2807–2824, Sep. 2014.

[19] J. Muller, J. Müller, F. Chen, R. Tetzlaff, J. Müller, E. Böhl, M. Kirsch, and C. Schnabel, "Registration and fusion of thermographic and visual-light images in neurosurgery," (in English), *IEEE Trans. Biomed. Circuits Syst.*, vol. 12, no. 6, pp. 1313–1321, Dec. 2018.

[20] F. Weidner, P. Urban, T. Meyer, C. Schnabel, Y. Radev, G. Schackert, U. Petersohn, E. Koch, S. Gumhold, G. Steiner, and M. Kirsch, "Framework for 2D-3D image fusion of infrared thermography with preoperative MRI," (in English), *Biomed. Eng.-Biomedizinische Technik*, vol. 62, no. 6, pp. 599–607, Dec. 2017.

[21] S. Wang, Z. Liu, P. Shen, and Q. Ji, "Eye localization from thermal infrared images," *Pattern Recognit.*, vol. 46, no. 10, pp. 2613–2621, 2013.

[22] Z. Hossein-Nejad and M. Nasri, "A-RANSAC: Adaptive random sample consensus method in multimodal retinal image registration," (in English), *Biomed. Signal Process. Control*, vol. 45, pp. 325–338, Aug. 2018.

[23] W. Birkfellner, M. Figl, H. Furtado, A. Renner, S. Hatamikia, and J. Hummel, "Multi-modality imaging: A software fusion and image-guided therapy perspective," (in English), *Frontiers Phys., Rev.*, vol. 6, p. 12, Jul. 17 2018, Art. no. 66.

[24] P. Viola and M. J. Jones, "Robust real-time face detection," (in English), *Int. J. Comput. Vis.*, vol. 57, no. 2, pp. 137–154, 2004.

[25] S. Z. Li and Z. Zhang, "FloatBoost learning and statistical face detection," *IEEE Trans. Pattern Anal. Mach. Intell.*, vol. 26, no. 9, pp. 1112–1123, Sep. 2004.

[26] S. Baskan, M. M. Bulut, and V. Atalay, "Projection based method for segmentation of human face and its evaluation," *Pattern Recognit. Lett.*, vol. 23, no. 14, pp. 1623–1629, 2002.

[27] G. C. Feng and P. C. Yuen, "Multi-cues eye detection on gray intensity image," *Pattern Recognit.*, vol. 34, no. 5, pp. 1033–1046, May 2001.

[28] C.-L. Chen and B.-L. Jian, "Infrared thermal facial image sequence registration analysis and verification," (in English), *Infr. Phys. Technol.*, vol. 69, pp. 1–6, Mar. 2015.

[29] M. Abdel-Basset, A. E. Fakhry, I. El-Henawy, T. Qiu, and A. K. Sangaiah, "Feature and intensity based medical image registration using particle swarm optimization," (in English), *J. Med. Syst.*, vol. 41, no. 12, p. 15, Nov. 2017, Art. no. 197.

[30] X. P. Liu, S. L. Chen, L. Zhuo, J. Li, and K. N. Huang, "Multisensor image registration by combining local self-similarity matching and mutual information," (in English), *Frontiers Earth Sci.*, vol. 12, no. 4, pp. 779–790, Dec. 2018.

[31] X. Wu, C. J. Li, Y. F. He, and W. L. Jia, "Operation optimization of natural gas transmission pipelines based on stochastic optimization algorithms: A review," (in English), *Math. Problems Eng.*, vol. 18, 2018, Art. no. 1267045.

[32] K. K. Castillo-Villar, "Metaheuristic algorithms applied to bioenergy supply chain problems: Theory, review, challenges, and future," (in English), *Energies, Rev.*, vol. 7, no. 11, pp. 7640–7672, Nov. 2014.

[33] H. R. Maier, S. Razavi, Z. Kapelan, L. S. Matott, J. Kasprzyk, and B. A. Tolson, "Introductory overview: Optimization using evolutionary algorithms and other metaheuristics," *Environ. Model. Softw.*, vol. 114, pp. 195–213, Apr. 2019.

[34] N. Masoumi, Y. Xiao, and H. Rivaz, "ARENA: Inter-modality affine registration using evolutionary strategy," (in English), *Int. J. Comput. Assist. Radiol. Surg.*, vol. 14, no. 3, pp. 441–450, Mar. 2019.

[35] P. J. Lang, M. M. Bradley, and B. N. Cuthbert, "International affective picture system (IAPS): Affective ratings of pictures and instruction manual," Univ. Florida, Gainesville, FL, USA, Tech. Rep. A-8, 2008.

[36] E. Rahtu and J. Heikkilä, "A Simple and efficient saliency detector for background subtraction," in *Proc. IEEE 12th Int. Conf. Comput. Vis. Workshops, ICCV Workshops*, Sep. 2009, pp. 1137–1144.

[37] M. S. G. Karypis, V. Kumar, and M. Steinbach, "A comparison of document clustering techniques," in *Proc. TextMining Workshop KDD*, May 2000, pp. 525–526.

[38] A. A. Goshtasby, *Image Registration: Principles, Tools and Methods*. London, U.K.: Springer, 2012.

[39] G.-A. Bilodeau, A. Torabi, P.-L. St-Charles, and D. Riahi, "Thermal-visible registration of human silhouettes: A similarity measure performance evaluation," *Infr. Phys. Technol.*, vol. 64, no. 0, pp. 79–86, 2014.

[40] Y. Ye and J. Shan, "A local descriptor based registration method for multispectral remote sensing images with non-linear intensity differences," *ISPRS J. Photogramm. Remote Sens.*, vol. 90, pp. 83–95, Apr. 2014.

[41] H. Rivaz, Z. Karimaghaloo, and D. L. Collins, "Self-similarity weighted mutual information: A new nonrigid image registration metric," *Med. Image Anal.*, vol. 18, no. 2, pp. 343–358, 2014.

[42] D. E. Goldberg, *Genetic Algorithms in Search, Optimization and Machine Learning*. Reading, MA, USA: Addison-Wesley, 1989, p. 372.

[43] A. R. Conn, I. M. G. Nicholas, and P. L. Toint, "A globally convergent augmented Langrangian algorithm for optimization with general constraints and simple bounds," *SIAM J. Numer. Anal.*, vol. 28, no. 2, pp. 545–572, 1991.
[44] A. R. Conn, N. Gould, and P. L. Toint, "A globally convergent Lagrangian barrier algorithm for optimization with general inequality constraints and simple bounds," (in English), *Math. Comput.*, vol. 66, no. 217, pp. 261–288, Jan. 1997.
[45] E. Mezura-Montes and C. A. Coello-Coello, "Constraint-handling in nature-inspired numerical optimization: Past, present and future," *Swarm Evol. Comput.*, vol. 1, no. 4, pp. 173–194, 2011.
[46] J. Kennedy and R. Eberhart, "Particle swarm optimization," in *Proc. Int. Conf. Neural Netw. ICNN*, vol. 4, 1995, pp. 1942–1948.
[47] M. E. H. Pedersen, "Good parameters for particle swarm optimization," Copenhagen, Denmark, Tech. Rep. HL1001, 2010.
[48] L. Ingber, "Simulated annealing applied to combinatorial optimization," Adaptive Simulated Annealing (ASA): Lessons Learned. Invited Paper to a Special Issue of the Polish Journal Control and Cybernetics, 1995.
[49] M. Sheikhalishahi, N. Eskandari, A. Mashayekhi, and A. Azadeh, "Multi-objective open shop scheduling by considering human error and preventive maintenance," (in English), *Appl. Math. Model.*, vol. 67, pp. 573–587, Mar. 2019.
[50] L. Yue, Z. Guan, L. Zhang, S. Ullah, and Y. Cui, "Multi objective lotsizing and scheduling with material constraints in flexible parallel lines using a Pareto based guided artificial bee colony algorithm," (in English), *Comput. Ind. Eng.*, vol. 128, pp. 659–680, Feb. 2019.
[51] K. Li, S. L. Yan, Y. C. Zhong, W. F. Pan, and G. Zhao, "Multi-objective optimization of the fiber-reinforced composite injection molding process using Taguchi method, RSM, and NSGA-II," (in English), *Simul. Model. Pract. Theory*, vol. 91, pp. 69–82, Feb. 2019.
[52] C. Li, C. Xu, C. Gui, and M. D. Fox, "Distance regularized level set evolution and its application to image segmentation," *IEEE Trans. Image Process.*, vol. 19, no. 12, pp. 3243–3254, Dec. 2010.
[53] Z. Wang, C.-S. Leung, T.-T. Wong, and Y.-S. Zhu, "Eigen-image based compression for the image-based relighting with cascade recursive least squared networks," *Pattern Recognit.*, vol. 37, no. 6, pp. 1219–1231, 2004.
[54] R.-Z. Wang, C.-F. Lin, and J.-C. Lin, "Image hiding by optimal LSB substitution and genetic algorithm," *Pattern Recognit.*, vol. 34, no. 3, pp. 671–683, 2001.
[55] A. S. Malik and T.-S. Choi, "A novel algorithm for estimation of depth map using image focus for 3D shape recovery in the presence of noise," *Pattern Recognit.*, vol. 41, no. 7, pp. 2200–2225, 2008.
[56] Z. Wang, A. C. Bovik, H. R. Sheikh, and E. P. Simoncelli, "Image quality assessment: From error visibility to structural similarity," *IEEE Trans. Image Process.*, vol. 13, no. 4, pp. 600–612, Apr. 2004.

BO-LIN JIAN received the B.S. degree from the Department of Electrical Engineering, National Formosa University, in 2009, the M.S. degree in materials science and engineering from the National Taiwan University of Science and Technology, in 2011, and the Ph.D. degree from the Department of Aeronautics and Astronautics, National Cheng Kung University, in 2017. He is currently an Assistant Professor with the Department of Electrical Engineering, National Chin-Yi University of Technology, Taichung, Taiwan. His current research interests include signal and image processing, machine learning, and control systems.

CHIEH-LI CHEN received the B.S. degree in mechanical engineering from National Taiwan University, Taipei, Taiwan, in 1983, and the M.S. and Ph.D. degrees in control engineering from the University of Manchester Institute of Science and Technology (UMIST), Manchester, U.K., in 1987 and 1989, respectively. He is currently a Professor with the Department of Aeronautics and Astronautics, National Cheng Kung University, Tainan, Taiwan, where he currently teaches in the areas of automatic control and machine vision. His research interests include automation, optimization, nonlinear dynamics, robust control, vibration and energy system management, and machine vision.

CHIH-JER LIN (M'12) received the B.S., M.S., and Ph.D. degrees from National Cheng Kung University, Tainan, Taiwan, in 1992, 1994, and 1998, respectively, all in mechanical engineering. He is currently an Associate Professor with the Graduate Institute of Automation and Technology, National Taipei University of Technology, Taipei, Taiwan. His current research interests include mechatronics, precision motion control, system identification, sliding-mode control, robotics, and evolutionary algorithms.

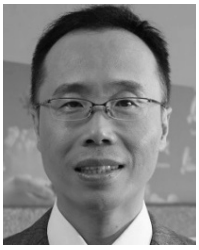

HER-TERNG YAU received the B.S. degree from the National Chung Hsing University, Taichung, Taiwan, in 1994, and the M.S. and Ph.D. degrees from the National Cheng Kung University, Tainan, Taiwan, in 1996 and 2000, respectively, all in mechanical engineering. He is currently a Professor with the Department of Electrical Engineering, National Chin-Yi University of Technology, Taichung. He is the author of more than 150 research articles on a wide variety of topics in mechanical and electrical engineering. His research interests include energy converter control, system control of mechatronics, nonlinear system analysis, and control.